HHS Public Access

Author manuscript

Radiat Res. Author manuscript; available in PMC 2015 December 22.

Published in final edited form as:

Radiat Res. 2015 June ; 183(6): 610–619. doi:10.1667/RR13979.1.

Effects of Local Heart Irradiation in a Glutathione S-Transferase Alpha 4-Null Mouse Model

Marjan Boerma[a,1], **Preeti Singh**[b], **Vijayalakshmi Sridharan**[a], **Preeti Tripathi**[a], **Sunil Sharma**[c], and **Sharda P. Singh**[b]

[a]Department of Pharmaceutical Sciences, Division of Radiation Health, University of Arkansas for Medical Sciences, Little Rock, Arkansas

[b]Departments of Pharmacology and Toxicology, University of Arkansas for Medical Sciences, Little Rock, Arkansas

[c]Department of Radiation Oncology, University of Arkansas for Medical Sciences, Little Rock, Arkansas

Abstract

Glutathione S-transferase alpha 4 (GSTA4-4) is one of the enzymes responsible for the removal of 4-hydroxynonenal (4-HNE), an electrophilic product of lipid peroxidation in cellular membranes during oxidative stress. 4-HNE is a direct activator of nuclear factor (erythroid-derived 2)-like 2 (Nrf2), a transcription factor with many target genes encoding antioxidant and anti-electrophile enzymes. We have previously shown that *Gsta4*-null mice on a 129/Sv background exhibited increased activity of Nrf2 in the heart. Here we examined the sensitivity of this *Gsta4*-null mouse model towards cardiac function and structure loss due to local heart irradiation. Male *Gsta4*-null and wild-type mice were exposed to a single X-ray dose of 18 Gy to the heart. Six months after irradiation, immunohistochemical staining for respiratory complexes 2 and 5 indicated that radiation exposure had caused most pronounced alterations in mitochondrial morphology in *Gsta4*-null mice. On the other hand, wild-type mice showed a decline in cardiac function and an increase in plasma levels of troponin-I, while no such changes were observed in *Gsta4*-null mice. Radiation-induced Nrf2-target gene expression only in *Gsta4*-null mice. In conclusion, although loss of GSTA4-4 led to enhanced susceptibility of cardiac mitochondria to radiation-induced loss of morphology, cardiac function was preserved in *Gsta4*-null mice. We propose that this protection against cardiac function loss may occur, at least in part, by upregulation of the Nrf2 pathway.

INTRODUCTION

Glutathione S-transferase alpha 4 (GSTA4-4) is one of the enzymes responsible for the removal of 4-hydroxynonenal (4-HNE), an electrophilic product of lipid peroxidation

[1]Address for correspondence: University of Arkansas for Medical Sciences, Department of Pharmaceutical Sciences, 4301 West Markham, Slot 522-10, Little Rock, AR 72205; mboerma@uams.edu.

Editor's note. The online version of this article (DOI: 10.1667/RR13979.1) contains supplementary information that is available to all authorized users.

formed in cellular membranes during oxidative stress, by conjugating it with glutathione (1). We have previously generated and characterized *Gsta4*-null mice on a 129/Sv and a C57BL genetic background (2, 3). When on a 129/Sv background, these mice show reduced glutathione conjugation of 4-HNE in all tissues examined, including the liver, kidney, lung and heart (2, 4). We previously detected increased activity of nuclear factor (erythroid-derived 2)-like 2 (Nrf2), a transcription factor that has many antioxidant and anti-electrophile enzyme target genes (5, 6), in the heart of *Gsta4*-null mice, and hypothesized that the lack of GSTA4-4 had caused a compensatory upregulation of the Nrf2 pathway (7).

Under normal conditions, Nrf2 is bound in the cytosol by its repressor, kelch-like ECH-associated protein 1 (Keap1), which targets Nrf2 for ubiquitination and degradation. Electrophilic stresses modify a cysteine residue of Keap1, which allows Nrf2 to escape degradation and translocate to the nucleus (8). Phosphoglycerate mutase family member 5 (PGAM5), which lacks typical phosphoglycerate mutase activity but contains a conserved phosphatase domain and exhibits serine-threonine phosphatase activity (9), is tethered to the mitochondrial outer membrane and may be involved in sensing oxidative status and activating Nrf2 (10).

Gsta4-null mice on a 129/Sv background show enhanced resistance to doxorubicin compared to wild-type animals, both in terms of survival and cardiac function loss (7). Because doxorubicin is known to be cardiotoxic at least in part due to induction of oxidative stress, these results suggest that compensatory mechanisms such as the Nrf2 pathway may have conveyed protection in the *Gsta4*-null mice. Doxorubicin, however, is administered systemically, and mechanisms outside the heart may have contributed to the protection of these *Gsta4*-null mice. In this study, we subjected the *Gsta4*-null mice on a 129/Sv background to local heart irradiation to produce oxidative stress locally in the heart. Since cardiac injury is known to occur late after exposure to ionizing radiation (11), long-term effects of local heart irradiation on cardiac function, structure and mitochondrial oxygen flux were examined.

MATERIALS AND METHODS

Animal Model

This study conformed to the Guide for the Care and Use of Laboratory Animals of the National Institutes of Health and was approved by the Institutional Animal Care and Use Committee. Male *Gsta4*-null mice on a 129/Sv background were obtained from a local breeding colony of homozygous *Gsta4*-null mice that had previously been generated (2). Matching wild-type mice were derived from breeding of heterozygous *Gsta4*-null mice to maintain the genetic background of wild-type animals. All mice were on a 12:12 h light-dark cycle with free access to water and chow (Teklad Lab LM-485; Harlan® Laboratories Inc., Indianapolis, IN). All animals were genotyped by performing a PCR on tail biopsy samples, as previously described (4).

Local Heart Irradiation

Image-guided local heart irradiation was performed with the Small Animal Conformal Radiation Therapy Device (SACRTD) at our institution as described for rats (12), but with the following modifications for our mouse model. Mice were exposed to local heart irradiation at 14 weeks of age. Mice were anesthetized with 3% isoflurane inhalation and placed vertically in a cylindrical Plexiglas® holder with an opening to allow direct contact between the radiation beam and the chest. The heart was exposed to X rays with three 5 mm diameter fields (anterior-posterior and two lateral fields) to 6 Gy each (225 kV, 13 mA, 0.5 mm Cu filtration, 1.92 Gy/min at 1 cm tissue depth) for a total of 18 Gy. Before each exposure, the location of the heart was verified with the X-ray imager (70 kV, 5 mA, <1 cGy). Dosimetry was performed as described previously (12). Experimental groups contained 5–8 mice.

Echocardiography

Echocardiography was performed with a Vevo 770 imaging system and RMV707B transducer (15–45 MHz) (VisualSonics Inc., Toronto, Canada) as previously described (9). Anesthesia was maintained with isoflurane at 2–3%, continuously adjusted so that heart rate remained at 360–420 beats per min. Short axis M-mode recordings at the mid-left ventricular level were used to obtain left ventricular wall thickness, inner diameter and volume, and the functional parameters of ejection fraction, fractional shortening, stroke volume and cardiac output.

Tissue Collection

Six months after local heart irradiation, mice were anesthetized by inhalation of 3% isoflurane, and a blood sample was collected from the abdominal aorta into Microtainer® tubes coated with EDTA. Blood was immediately centrifuged at 1,000*g* for 15 min at 4°C, and the supernatant was collected and centrifuged at 10,000*g* for 5 min to collect plasma for measurements of cardiac troponin-I (cTnI).

Hearts were briefly rinsed in PBS and cut longitudinally with one-half fixed in 10% buffered formalin to obtain tissue sections of both the left and right ventricles. Tissues were processed for histology and immunohistochemistry as described below. An additional longitudinal piece of the left ventricle (~50 mg) was placed on ice for immediate analysis of tissue oxygen consumption with respirometry, as described below. Remaining tissue specimens were snap-frozen in liquid nitrogen for molecular and biochemical analyses.

Determination of Plasma Cardiac Troponin-I Levels

A mouse cTnI ELISA kit from Life Diagnostics, Inc. (West Chester, PA) was used to assess troponin levels in 100 μl of plasma, according to manufacturer's instructions. The concentration of cTnI was detected by reading the absorbance at 450 nm.

Histology

Formalin-fixed tissue specimens were processed, embedded in paraffin and 5 μm sections were obtained for histology or immunohistochemistry.

For determination of collagen deposition, sections were rehydrated and incubated in Sirius red (American MasterTech Scientific, Lodi, CA) supplemented with fast green (Fisher Scientific™, Waltham, MA) for 1 h, followed by 0.5% acetic acid for 14 min. The stained sections were examined with a ScanScope CS2 slide scanner and analyzed with ImageScope 12 software (Aperio®, Vista, CA). The area stained positive with Sirius red was determined and calculated as the percentage of the total tissue area of each section.

For determination of mast cell numbers, sections were rehydrated and incubated in 0.5% toluidine blue in 0.5 *N* HCl for 72 h, followed by 0.7 *N* HCl for 10 min. Stained sections were examined with an Axioskop transmitted light microscope (Carl Zeiss, Oberkochen, Germany), and the mast cells in each section were counted.

For determination of apoptotic nuclei, the CardioTACS™ kit (Trevigen®, Gaithersburg, MD), which is based on DNA end labeling with terminal deoxynucleotidyl transferase (TUNEL-like assay), was used according to the manufacturer's instructions. Stained sections were examined with an Axioskop transmitted light microscope (Carl Zeiss) and the apoptotic nuclei in the ventricles of each heart section were counted.

Lectin staining was used to determine microvascular density. Sections were deparaffinated and rehydrated, and antigen retrieval was performed by treating the sections with 10 m*M* sodium citrate pH 6.0 at 95°C for 20 min. Sections were allowed to cool down prior to incubation in 1% H_2O_2 in methanol for 30 min to quench the endogenous peroxidase activity. Sections were subsequently incubated with biotinylated Lycopersicon esculentum (tomato) lectin (1:200; Vector Laboratories, Burlingame, CA) for 90 min at room temperature. Lectin staining was visualized by incubating the sections in avidin-biotin-peroxidase complex (Vector Laboratories) for 45 min at room temperature and then in DAB (Sigma-Aldrich® LLC, St. Louis, MO). Counter staining was done by hematoxylin followed by dehydrating and mounting. Stained sections were examined using a Zeiss AxioImager M2 microscope and Neurolucida 64 bit and Neurolucida Explorer software (MBF Bioscience, Williston, VT). Four to six fields were randomly selected to count the lectin stained capillaries at 40× magnification in each section, and the total numbers of capillaries were divided by the area of the field to obtain capillary density. The average value of capillary density of each section was used as a single data point for statistical analysis.

Immunohistochemistry

For immunohistochemical analysis of mitochondrial complexes, sections were treated for antigen retrieval and quenching of endogenous peroxidase as described above. Sections were stained using the Animal Research Kit (ARK™) Peroxidase (Dako, Glostrup, Denmark) following the manufacturer's instructions with minor modifications. In short, mouse anti-complex II IgG (1:100; Life Technologies, Grand Island, NY) or mouse anti-ATP synthase subunit beta IgG (1:100, Life Technologies) was mixed with modified biotinylated anti-mouse immunoglobulin and normal mouse serum, and sections were incubated with the antibodies for 1 h at room temperature, followed by streptavidin-peroxidase for 15 min and 3,3′-diaminobenzidine chromogen solution for 5 min (Dako). Hematoxylin was used as a counterstain.

Western Blot Analysis

A portion of heart tissue was homogenized in RIPA buffer (50 m*M* tris, pH 8.0; 150 m*M* NaCl; 0.2 m*M* EDTA; 1% Nonidet P-40; 0.5% sodium deoxycholate) supplemented with 1× protease and phosphatase inhibitor mixture (Roche Applied Science, Indianapolis, IN) and centrifuged for 15 min at 15,000×g. A total of 25 μg of protein, prepared in Laemmli sample buffer containing β-mercaptoethanol (1:20 vol/vol) and boiled for 2–3 min, was separated in Any kD™ Mini-Protean® polyacrylamide or 4–20% TGX Mini-Protean® polyacrylamide gels and transferred to polyvinylidene fluoride membranes (Bio-Rad Laboratories Inc., Hercules, CA). Nonspecific antibody binding was reduced by tris-buffered saline (TBS) containing 0.05% Tween®-20 and 5% nonfat dry milk. Membranes were then incubated overnight at 4°C or for 1 h at room temperature with primary antibodies (listed in Supplementary Table S1; http://dx.doi.org/10.1667/RR13979.1.S1), all in TBS containing 5% nonfat dry milk and 0.1% Tween-20, followed by HRP-conjugated secondary antibodies (Supplementary Table S1). Antibody binding was visualized using the Western blotting detection reagent, ECL Plus (GE Healthcare Life Sciences, Logan, UT) on CL-Xposure™ film (Thermo Scientific, Waltham, MA). Films were scanned using an AlphaImager® gel documentation system (ProteinSimple®, Santa Clara, CA) and protein bands were quantified with ImageJ software (NIH, Bethesda, MD). Protein loading was corrected by dividing the target protein band density by that of GAPDH.

Tissue Oxygen Flux by High-Resolution Respirometry

High-resolution respirometry was performed on freshly isolated tissue samples from the left ventricle as described elsewhere (13, 14). Briefly, myocardial tissue samples were permeabilized by gentle agitation in relaxing solution supplemented with 50 mg/ml saponin for 30 min at 4°C, followed by washing in ice-cold respiration media for 10 min. Fibers were maintained in this media until the start of the respirometric assay in an oxygraph (Oroboros Instruments, Innsbruck, Austria). Oxygen flux was measured at 37°C using a substrate inhibitor titration protocol as described by the oxygraph manufacturer. Complex I activity was tested by addition of the substrates malate (2 m*M*) and glutamate (10 m*M*) to initiate the respiration, followed by 2.5 m*M* ADP to achieve maximal respiration. Subsequently, complex I was inhibited by the addition of 0.2 m*M* rotenone. Complex II/III respiration was stimulated by the addition of 10 m*M* succinate, followed by the addition of complex III inhibitor antimycin A (10 μ*M*). Lastly, complex IV respiration was measured by addition of 1 m*M* N,N,N′,N′-tetramethyl-p-phenylenediamine (TMPD) made in 0.8 *M* ascorbate (pH = 6.0), and complex IV activity was then inhibited by adding 800 m*M* sodium azide. Data acquisition and analysis was performed using DatLab 4.2 software (Oroboros Instruments). Respiratory rates were expressed per mg tissue weight.

Determination of mRNA Levels by Quantitative Real-Time Polymerase Chain Reaction

Total RNA was isolated from snap-frozen heart samples with a guanidinium thiocyanate method, using the FastRNA® Pro Green Kit (MP Biomedicals LLC, Santa Ana, CA). Complementary DNA was prepared using the Verso cDNA Synthesis Kit (Thermo Scientific™, Pittsburgh, PA), in accordance with the supplier's instruction manual.

Reverse transcription real-time polymerase chain reactions (RT-qPCR) were performed on a DNA Engine Opticon® 2 Detection System (MJ Research, Waltham, MA) with the SYBR® select master mix (Applied Biosystems; Life Technologies) in a total volume of 20 μl containing 0.3 μ*M* gene-specific primers (Supplementary Table S2; http://dx.doi.org/10.1667/RR13979.1.S1). The ribosomal protein S3 transcript was used as a reference for normalization of mRNA levels (3) and relative mRNA values were calculated with the ΔΔCt method.

In Vitro Irradiation and Survival of Mouse Embryonic Fibroblasts

Embryonic fibroblasts were harvested from wild-type and *Gsta4*-null mice according to the method described previously (15). A single cell suspension was obtained in complete Dulbecco's modified Eagle media (DMEM) supplemented with penicillin and streptomycin and plated to obtain adhering mouse embryonic fibroblasts, which were cultured until 80–85% confluent and passaged at a ratio of 1:2. Primary cell cultures were maintained under standard culture conditions until colonies of spontaneously transformed cells appeared. Expression level of GSTA4-4 in wild-type and absence in *Gsta4*-null mouse embryonic fibroblasts was verified by Western blot analysis using an anti-mGSTA4-4 antibody produced in-house (2). A standard clonogenic assay (16) was performed on the wild-type and *Gsta4*-null immortalized mouse embryonic fibroblasts in triplicate to determine survival in response to Cs-137 gamma-ray exposure at doses of 3 and 6 Gy, at a dose rate of 1.8 Gy/min.

Statistical Analysis

Data are presented as average ± standard error of the mean (SEM). Statistical analysis was performed with the NCSS 8 software package (NCSS LLC, Kaysville, UT). Data were evaluated with two-way ANOVA, followed by Newman-Keuls individual comparisons. The criterion for significance was $P < 0.05$.

RESULTS

Effects of Local Heart Irradiation on Cardiac Function, Histology and Circulating cTnI

Gsta4-null mice show age-related obesity (4). However, our study was performed at an age when obesity was not yet apparent and there were no significant differences in bodyweight among the experimental groups (data not shown).

The thickness of the anterior and posterior walls of the left ventricle in systole in sham-irradiated *Gsta4*-null mice (1.93 ± 0.06 mm and 1.54 ± 0.05 mm, respectively, measured at 6 months after sham irradiation) was slightly but significantly increased compared to sham-irradiated wild-type mice (1.53 ± 0.09 mm and 1.23 ± 0.06 mm, respectively, $P < 0.05$). The difference in thickness of the left ventricular posterior wall persisted in the irradiated groups: at 6 months after local heart irradiation, a small but significant increase in left ventricular posterior wall thickness in systole was observed in *Gsta4*-null mice (1.48 ± 0.06 mm) compared to wild-type mice (1.22 ± 0.07 mm, $P < 0.05$). Moreover, while exposure to radiation caused a significant reduction in ejection fraction (data not shown), stroke volume, fractional shortening and cardiac output in wild-type animals, the *Gsta4*-null mice appeared

to be protected against these effects (Fig. 1). Reductions in cardiac function parameters in irradiated wild-type mice were associated with increased plasma levels of the cardiac disease marker cTnI in this group only (Fig. 1).

Local heart irradiation has been shown to cause mild fibrosis and a reduction in cardiac capillary density in some mouse strains (17). In this study, local heart irradiation did not induce a change in collagen deposition at the 6 month time point (data not shown). Although radiation exposure reduced capillary density in both genotypes, the difference was significant only in wild-type mice. Lastly, cardiac mast cell numbers were significantly reduced in irradiated *Gsta4*-null mice (Fig. 2).

Effects of Local Heart Irradiation on Markers of Apoptosis

At 6 months after local heart irradiation, wild-type mice showed no significant changes in left ventricular Bax and Bcl2 levels (Supplementary Fig. S1; http://dx.doi.org/10.1667/RR13979.1.S1), cleaved caspase-3 or the number of apoptotic nuclei (Fig. 3). In *Gsta4*-null mice, a significant increase was seen in levels of the anti-apoptotic protein Bcl2 (Supplementary Fig. S1). Three out of five irradiated *Gsta4*-null mice showed a clear increase in cleaved caspase-3 (Fig. 3). Nonetheless, and seemingly discrepant with the caspase-3 results, significantly fewer apoptotic nuclei were detected in both sham-irradiated and irradiated *Gsta4*-null compared to wild-type mice (Fig. 3).

Effects of Gsta4 Deletion and Local Heart Irradiation on Nrf2 Target Genes

We previously showed that *Gsta4*-null mice on a 129/Sv genetic background exhibit a higher baseline activity of the Nrf2 pathway in the heart (9). Therefore, in this study, we examined the expression of *Nrf2, PGAM5* and a number of Nrf2 target genes in response to radiation exposure. mRNA levels for both *Nrf2* and *PGAM5* were significantly higher in *Gsta4*-null mice (Table 1). We also found a fourfold increase in Nrf2 protein level in the left ventricle of sham-irradiated *Gsta4*-null mice compared to wild-type mice (Supplementary Fig. S2; http://dx.doi.org/10.1667/RR13979.1.S1). Next, we investigated the expression of 14 target genes of the Nrf2 pathway and found that, while none were significantly altered by radiation exposure in wild-type mice, 7 genes were significantly upregulated in *Gsta4*-null mice, with fold changes between 1.59 and 3.05 in irradiated *Gsta4*-null mice compared to sham-irradiated *Gsta4*-null mice ($P < 0.05$, Table 1). Western blots were used to verify the radiation-induced increase in expression of the Nrf2 targets superoxide dismutase 2 (SOD2) and glutathione peroxidase 1 (Gpx1) in *Gsta4*-null mice (Fig. 4). Together, these results suggest that there was a stronger induction of the Nrf2 pathway upon irradiation in the *Gsta4*-null mice.

Effects of Gsta4 Deletion and Local Heart Irradiation on Mitochondrial Properties

Exposure to ionizing radiation has been shown to modify cardiac mitochondrial morphology and function (18). Figure 5 contains representative images of immunohistochemical analysis of mitochondrial respiratory chain complexes 2 and 5. While local heart irradiation did not induce a change in the staining pattern of these complexes in wild-type mice, staining in irradiated *Gsta4*-null mice was reduced. This difference was observed throughout the heart of the irradiated *Gsta4*-null mice, indicated by a change in staining pattern in both ventricles

and atria (Fig. 5). To determine whether the reduction in complex 2 and 5 immunostaining was due to a reduction in protein expression, or potentially a change in mitochondrial morphology, we next examined complex 2 and 5 expression by Western blot analysis. While complex 2 expression was not significantly altered in any of the groups, a significant increase was observed in complex 5 expression in irradiated *Gsta4*-null mice (Supplementary Fig. S3; http://dx.doi.org/10.1667/RR13979.1.S1). Therefore, the changes in tissue pattern of complexes 2 and 5 in irradiated *Gsta4*-null mice may indicate that a change in mitochondrial morphology had occurred.

To further assess the effects of local heart irradiation on mitochondria, we examined left ventricular tissue oxygen flux through individual respiratory complexes at the 6 month time point. *Gsta4*-null mice showed an increased oxygen flux through complexes 1, 2 and 3. Local heart irradiation caused a small but significant increase in oxygen flux through complexes 2 and 3 in wild-type mice and a small decrease in *Gsta4*-null mice. Nonetheless, oxygen flux in irradiated *Gsta4*-null hearts was still significantly higher compared to irradiated wild-type hearts (Fig. 6).

Effects of In Vitro Irradiation on Mouse Embryonic Fibroblast Survival

To test whether *Gsta4* deletion caused an inherent cellular resistance to ionizing radiation, we examined survival of immortalized mouse embryonic fibroblasts in response to γ rays in culture. Although exposure to radiation caused reduced survival in mouse embryonic fibroblasts of both genotypes, survival was significantly higher in those embryonic fibroblasts isolated from *Gsta4*-null mice compared to wild-type mouse embryonic fibroblasts (Fig. 7).

DISCUSSION

This study examined the long-term effects of local heart irradiation in *Gsta4*-null and wild-type mice on a 129/Sv genetic background. Altogether, our results suggest that *Gsta4*-null mice show a compensatory upregulation of the Nrf2 pathway and are therefore more resistant against a radiation-induced cardiac function loss compared to wild-type mice. We have previously observed a similar result with doxorubicin cardiotoxicity (7). These results emphasize that a gene knockout may lead to the induction of compensation mechanisms, thereby complicating the conclusions drawn on the role of the gene of interest.

Local heart irradiation has previously been shown to induce mild delayed cardiac fibrosis and reduced capillary density in certain mouse strains (17). Here we did not observe an effect of radiation on cardiac collagen deposition, suggesting that the genetic background of the mice in this study may not be prone to radiation-induced fibrosis. Reduced capillary density, on the other hand, was observed but was only statistically significant in the irradiated wild-type mice, suggesting that there was some protection in *Gsta4*-null mice. The heart contains a low number of mast cells, which may play an important role in cardiac remodeling (19–21). We have previously shown that in animal models of local heart irradiation, cardiac resident mast cells reduce in number within the first weeks postirradiation, followed by significantly increased numbers at months after irradiation, correlating with adverse myocardial remodeling (22). The early reduction in mast cell

number may be a direct response of the mast cells to radiation exposure. In the current experiment, *Gsta4*-null mice showed significantly reduced cardiac mast cell numbers at 6 months after local heart irradiation. It may be possible that upon early loss of cardiac mast cells, *Gsta4*-null mice do not activate the mechanisms required to induce cardiac mast cell infiltration. The biological implications of the reduced mast cell numbers in the *Gsta4*-null mice require further examination.

GSTA4-4 catalyzes the glutathione conjugation of 4-HNE. We have previously shown reduced glutathione conjugated 4-HNE in *Gsta4*-null mice on a 129/Sv background, in organs that normally show a high expression of GSTA4-4, such as the heart (2). Through its electrophilic properties, 4-HNE directly activates Nrf2, a transcription factor that induces the expression of an array of antioxidant enzyme genes (5). Here we show that a large number of Nrf2 target genes are significantly upregulated 1.6- to 3-fold in response to local heart irradiation only in *Gsta4*-null mice. Moreover, in addition to reduced radiation-induced cardiac function loss in *Gsta4*-null mice, embryonic fibroblasts isolated from *Gsta4*-null mice showed increased survival after exposure to radiation compared to wild-type mouse embryonic fibroblasts, suggesting that cells of *Gsta4*-null mice may show an inherent resistance to radiation. We have previously shown that *Gsta4*-null mouse embryonic fibroblasts were more susceptible to injury and cell death when treated with oxidants for 24 h (15). However, it is likely that the conditions in the previous experiments led to higher oxidant concentrations and longer exposure to oxidants than in the current study with ionizing radiation.

Previous studies have shown prolonged alterations in mitochondrial respiration in animal models of local heart irradiation, both when isolated mitochondria and cardiac tissue homogenates were examined (18, 23–25). Here, we used a tissue oxygraph to determine oxygen consumption through the various mitochondrial respiratory complexes in the left ventricular tissue. Oxygen flux through complexes 1, 2 and 3 was enhanced in sham-irradiated *Gsta4*-null mice compared to wild-type mice. Although we cannot confirm that the increase in oxygen flux coincided with an increase in oxidative phosphorylation, Nrf2 has recently been shown to promote mitochondrial respiration (26, 27). Therefore, increased Nrf2 activity could potentially be the cause of increased oxygen flux in *Gsta4*-null mice. A small but significant reduction in oxygen flux occurred only in irradiated *Gsta4*-null mice. The reduction in oxygen flux coincided with a compromised mitochondrial complex expression pattern, suggesting that radiation had a relatively more severe deleterious effect on cardiac mitochondria in this genotype. GSTA4-4 plays a role in modulating oxidative stress in mitochondria (28, 29). Apparently, while the GSTA4-4 deficiency in our mouse model led to a compensatory upregulation of the Nrf2 pathway and protection against radiation-induced cardiac function loss, the cardiac mitochondria seemed more susceptible to radiation-induced injury. In accordance with this observation, we have recently shown that modification of cardiac mitochondrial function is not directly related to a change in cardiac morphology or function in our animal models of local heart irradiation (unpublished data).

Although previous studies have demonstrated radiation-induced apoptosis in animal models of local heart irradiation (30, 31), we typically do not observe large numbers of apoptotic

cells at the 6 month time point in experiments with local heart irradiation in rat and mouse models (18). In accordance with our previous studies, radiation did not modify the number of apoptotic cells in wild-type mice. Interestingly, some increase in cardiac levels of cleaved caspase-3 was seen in irradiated *Gsta4*-null mice. Since caspase activation is downstream of mitochondrial alterations, these results corroborate the observation that radiation caused changes in mitochondrial morphology only in *Gsta4*-null mice. Nonetheless, a TUNEL-like staining revealed lower numbers of apoptotic cells in both sham-irradiated and irradiated *Gsta4*-null compared to wild-type mice. These seemingly discrepant results suggest that the induction of cleaved caspase-3 was not sufficient to cause apoptosis, and/or that anti-apoptotic signals, potentially via the Nrf2 pathway (32), may persevere in both sham-irradiated and irradiated *Gsta4*-null mice.

Altogether, our data suggest that *Gsta4*-null mice may be protected against radiation-induced cardiac injury at least in part by upregulation of the Nrf2 pathway. Indeed, since free 4-HNE levels are relatively high in the heart compared to other organs, one may expect a high activity of Nrf2 in the heart (33). Studies have begun to identify roles for Nrf2 in protection against radiation-induced injury in a variety of organ systems. In addition to inducing the expression of antioxidant enzymes, other detoxifying enzymes and cytoprotective proteins such as Bcl2, Nrf2 may also reduce inflammatory mediators, and activate Notch signaling in hematopoietic stem cells (8, 32, 34–43). The role of Nrf2 in radiation-induced cardiac injury needs to be further explored.

Supplementary Material

Refer to Web version on PubMed Central for supplementary material.

Acknowledgments

This work was supported in part by the National Institutes of Health (AG032643 to SPS and CA148679 to MB) and a grant from American Heart Association (14GRNT18890084 to SPS). The authors would like to thank Lee Ann MacMillan-Crow, Ph.D. and Nirmala Parajuli, Ph.D. for their advice on study design and experimental protocols and Helen Beneš, Ph.D. for her expert editing of the manuscript.

References

1. Hiratsuka A, Tobita K, Saito H, Sakamoto Y, Nakano H, Ogura K, et al. (S)-preferential detoxification of 4-hydroxy-2(E)-nonenal enantiomers by hepatic glutathione S-transferase isoforms in guinea-pigs and rats. Biochem J. 2001; 355:237–44. [PubMed: 11256969]
2. Engle MR, Singh SP, Czernik PJ, Gaddy D, Montague DC, Ceci JD, et al. Physiological role of mGSTA4-4, a glutathione S-transferase metabolizing 4-hydroxynonenal: generation and analysis of mGsta4 null mouse. Toxicol Appl Pharmacol. 2004; 194:296–308. [PubMed: 14761685]
3. Singh SP, Niemczyk M, Saini D, Sadovov V, Zimniak L, Zimniak P. Disruption of the mGsta4 gene increases life span of C57BL mice. J Gerontol A Biol Sci Med Sci. 2010; 65:14–23. [PubMed: 19880816]
4. Singh SP, Niemczyk M, Saini D, Awasthi YC, Zimniak L, Zimniak P. Role of the electrophilic lipid peroxidation product 4-hydroxynonenal in the development and maintenance of obesity in mice. Biochemistry. 2008; 47:3900–11. [PubMed: 18311940]
5. Chen ZH, Saito Y, Yoshida Y, Sekine A, Noguchi N, Niki E. 4-Hydroxynonenal induces adaptive response and enhances PC12 cell tolerance primarily through induction of thioredoxin reductase 1 via activation of Nrf2. J Biol Chem. 2005; 280:41921–7. [PubMed: 16219762]

6. Sykiotis GP, Bohmann D. Stress-activated cap'n'collar transcription factors in aging and human disease. Sci Signal. 2010; 3:re3. [PubMed: 20215646]
7. Benes H, Vuong MK, Boerma M, McElhanon KE, Siegel ER, Singh SP. Protection from oxidative and electrophilic stress in the Gsta4-null mouse heart. Cardiovasc Toxicol. 2013; 13:347–56. [PubMed: 23690225]
8. Kaspar JW, Niture SK, Jaiswal AK. Nrf2:INrf2 (Keap1) signaling in oxidative stress. Free Radic Biol Med. 2009; 47:1304–9. [PubMed: 19666107]
9. Takeda K, Komuro Y, Hayakawa T, Oguchi H, Ishida Y, Murakami S, et al. Mitochondrial phosphoglycerate mutase 5 uses alternate catalytic activity as a protein serine/threonine phosphatase to activate ASK1. Proc Natl Acad Sci U S A. 2009; 106:12301–5. [PubMed: 19590015]
10. Lo SC, Hannink M. PGAM5 tethers a ternary complex containing Keap1 and Nrf2 to mitochondria. Exp Cell Res. 2008; 314:1789–803. [PubMed: 18387606]
11. Lee MS, Finch W, Mahmud E. Cardiovascular complications of radiotherapy. Am J Cardiol. 2013; 112:1688–96. [PubMed: 24012026]
12. Sharma S, Moros EG, Boerma M, Sridharan V, Han EY, Clarkson R, et al. A novel technique for image-guided local heart irradiation in the rat. Technol Cancer Res Treat. 2014; 13:593–603. [PubMed: 24000983]
13. Kuznetsov AV, Schneeberger S, Seiler R, Brandacher G, Mark W, Steurer W, et al. Mitochondrial defects and heterogeneous cytochrome c release after cardiac cold ischemia and reperfusion. Am J Physiol Heart Circ Physiol. 2004; 286:H1633–41. [PubMed: 14693685]
14. Hughey CC, Hittel DS, Johnsen VL, Shearer J. Respirometric oxidative phosphorylation assessment in saponin-permeabilized cardiac fibers. J Vis Exp. 2011; 48:1–7.
15. McElhanon KE, Bose C, Sharma R, Wu L, Awasthi YC, Singh SP. Null mouse embryonic fibroblasts exhibit enhanced sensitivity to oxidants: role of 4-hydroxynonenal in oxidant toxicity. Open J Apoptosis. 2013; 2
16. Franken NA, Rodermond HM, Stap J, Haveman J, van BC. Clonogenic assay of cells in vitro. Nat Protoc. 2006; 1:2315–9. [PubMed: 17406473]
17. Seemann I, Gabriels K, Visser NL, Hoving S, te Poele JA, Pol JF, et al. Irradiation induced modest changes in murine cardiac function despite progressive structural damage to the myocardium and microvasculature. Radiother Oncol. 2012; 103:143–50. [PubMed: 22112779]
18. Sridharan V, Aykin-Burns N, Tripathi P, Krager KJ, Sharma SK, Moros EG, et al. Radiation-induced alterations in mitochondria of the rat heart. Radiat Res. 2014; 181:324–34. [PubMed: 24568130]
19. Boerma M, Wang J, Wondergem J, Joseph J, Qiu X, Kennedy RH, et al. Influence of mast cells on structural and functional manifestations of radiation-induced heart disease. Cancer Res. 2005; 65:3100–7. [PubMed: 15833839]
20. Estensen RD. What is the role of myocardial mast cells? Hum Pathol. 1985; 16:536–8. [PubMed: 3158583]
21. Sperr WR, Bankl HC, Mundigler G, Klappacher G, Grossschmidt K, Agis H, et al. The human cardiac mast cell: localization, isolation, phenotype, and functional characterization. Blood. 1994; 84:3876–84. [PubMed: 7524750]
22. Boerma M, Zurcher C, Esveldt I, Schutte-Bart CI, Wondergem J. Histopathology of ventricles, coronary arteries and mast cell accumulation in transverse and longitudinal sections of the rat heart after irradiation. Oncol Rep. 2004; 12:213–9. [PubMed: 15254680]
23. Barjaktarovic Z, Schmaltz D, Shyla A, Azimzadeh O, Schulz S, Haagen J, et al. Radiation-induced signaling results in mitochondrial impairment in mouse heart at 4 weeks after exposure to x-rays. PLoS One. 2011; 6:e27811. [PubMed: 22174747]
24. Barjaktarovic Z, Shyla A, Azimzadeh O, Schulz S, Haagen J, Dorr W, et al. Ionising radiation induces persistent alterations in the cardiac mitochondrial function of C57BL/6 mice 40 weeks after local heart exposure. Radiother Oncol. 2013; 106:404–10. [PubMed: 23522698]
25. Franken NA, Hollaar L, Bosker FJ, Van Ravels FJ, van der Laarse A, Wondergem J. Effects of in vivo heart irradiation on myocardial energy metabolism in rats. Radiat Res. 1993; 134:79–85. [PubMed: 8475257]

26. Ludtmann MH, Angelova PR, Zhang Y, Abramov AY, Dinkova-Kostova AT. Nrf2 affects the efficiency of mitochondrial fatty acid oxidation. Biochem J. 2014; 457:415–24. [PubMed: 24206218]
27. Holmstrom KM, Baird L, Zhang Y, Hargreaves I, Chalasani A, Land JM, et al. Nrf2 impacts cellular bioenergetics by controlling substrate availability for mitochondrial respiration. Biol Open. 2013; 2:761–70. [PubMed: 23951401]
28. Raza H, Robin MA, Fang JK, Avadhani NG. Multiple isoforms of mitochondrial glutathione S-transferases and their differential induction under oxidative stress. Biochem J. 2002; 366:45–55. [PubMed: 12020353]
29. Robin MA, Prabu SK, Raza H, Anandatheerthavarada HK, Avadhani NG. Phosphorylation enhances mitochondrial targeting of GSTA4-4 through increased affinity for binding to cytoplasmic Hsp70. J Biol Chem. 2003; 278:18960–70. [PubMed: 12646569]
30. Salata C, Ferreira-Machado SC, de Andrade CB, Mencalha AL, Mandarim-De-Lacerda CA, de Almeida CE. Apoptosis induction of cardiomyocytes and subsequent fibrosis after irradiation and neoadjuvant chemotherapy. Int J Radiat Biol. 2014; 90:284–90. [PubMed: 24467328]
31. Dogan I, Sezen O, Sonmez B, Zengin AY, Yenilmez E, Yulug E, et al. Myocardial perfusion alterations observed months after radiotherapy are related to the cellular damage. Nuklearmedizin. 2010; 49:209–15. [PubMed: 20949225]
32. Niture SK, Jaiswal AK. Nrf2 protein up-regulates antiapoptotic protein Bcl-2 and prevents cellular apoptosis. J Biol Chem. 2012; 287:9873–86. [PubMed: 22275372]
33. Zhang Y, Sano M, Shinmura K, Tamaki K, Katsumata Y, Matsuhashi T, et al. 4-hydroxy-2-nonenal protects against cardiac ischemia-reperfusion injury via the Nrf2-dependent pathway. J Mol Cell Cardiol. 2010; 49:576–86. [PubMed: 20685357]
34. Anuranjani Bala M. Concerted action of Nrf2-ARE pathway, MRN complex, HMGB1 and inflammatory cytokines - Implication in modification of radiation damage. Redox Biol. 2014; 2:832–46. [PubMed: 25009785]
35. Mathew ST, Bergstrom P, Hammarsten O. Repeated Nrf2 stimulation using sulforaphane protects fibroblasts from ionizing radiation. Toxicol Appl Pharmacol. 2014; 276:188–94. [PubMed: 24603300]
36. Kim JH, Thimmulappa RK, Kumar V, Cui W, Kumar S, Kombairaju P, et al. NRF2-mediated Notch pathway activation enhances hematopoietic reconstitution following myelosuppressive radiation. J Clin Invest. 2014; 124:730–41. [PubMed: 24463449]
37. Kim SB, Pandita RK, Eskiocak U, Ly P, Kaisani A, Kumar R, et al. Targeting of Nrf2 induces DNA damage signaling and protects colonic epithelial cells from ionizing radiation. Proc Natl Acad Sci U S A. 2012; 109:E2949–55. [PubMed: 23045680]
38. Kato K, Takahashi K, Monzen S, Yamamoto H, Maruyama A, Itoh K, et al. Relationship between radiosensitivity and Nrf2 target gene expression in human hematopoietic stem cells. Radiat Res. 2010; 174:177–84. [PubMed: 20681784]
39. Chute JP. NRF2 mitigates radiation-induced hematopoietic death. J Clin Invest. 2014; 124:960–1. [PubMed: 24569364]
40. Mathew B, Jacobson JR, Siegler JH, Moitra J, Blasco M, Xie L, et al. Role of migratory inhibition factor in age-related susceptibility to radiation lung injury via NF-E2-related factor-2 and antioxidant regulation. Am J Respir Cell Mol Biol. 2013; 49:269–78. [PubMed: 23526214]
41. McDonald JT, Kim K, Norris AJ, Vlashi E, Phillips TM, Lagadec C, et al. Ionizing radiation activates the Nrf2 antioxidant response. Cancer Res. 2010; 70:8886–95. [PubMed: 20940400]
42. Travis EL, Rachakonda G, Zhou X, Korhonen K, Sekhar KR, Biswas S, et al. NRF2 deficiency reduces life span of mice administered thoracic irradiation. Free Radic Biol Med. 2011; 51:1175–83. [PubMed: 21712086]
43. Rana T, Schultz MA, Freeman ML, Biswas S. Loss of Nrf2 accelerates ionizing radiation-induced bone loss by upregulating RANKL. Free Radic Biol Med. 2012; 53:2298–307. [PubMed: 23085426]

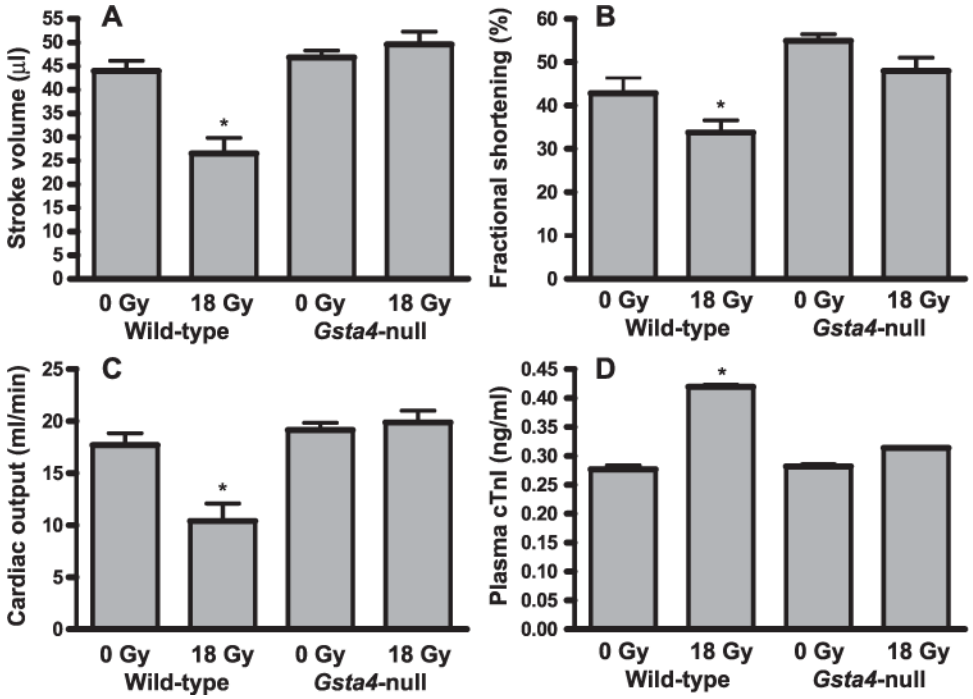

FIG. 1.

Echocardiographic parameters and plasma troponin I (cTnI) levels measured 6 months after local heart irradiation. Exposure to radiation caused a significant reduction in stroke volume (panel A), fractional shortening (panel B) and cardiac output (panel C), together with a significant increase in plasma cTnI levels (panel D) only in wild-type mice. Average ± SEM, n = 5–8. *$P < 0.05$ when compared to wild-type sham-irradiated mice.

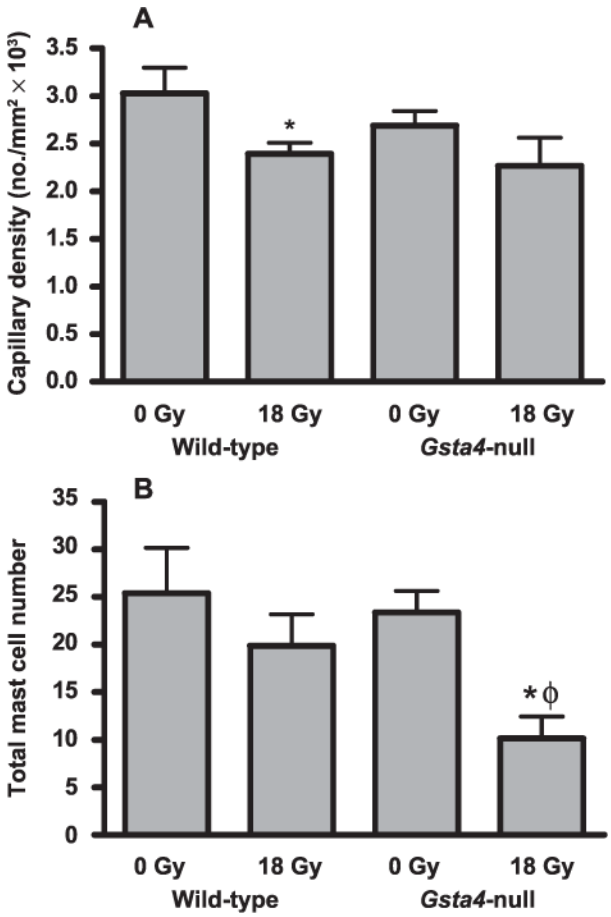

FIG. 2.

Histological parameters at 6 months after local heart irradiation. Panel A: Irradiation significantly reduced the capillary density in wild-type mice. Panel B: Cardiac mast cell numbers were significantly reduced only in irradiated *Gsta4*-null mice. Average ± SEM, n = 5–8. **P* < 0.05 when compared to wild-type sham-irradiated mice. φ*P* < 0.05 when compared to *Gsta4*-null sham-irradiated mice.

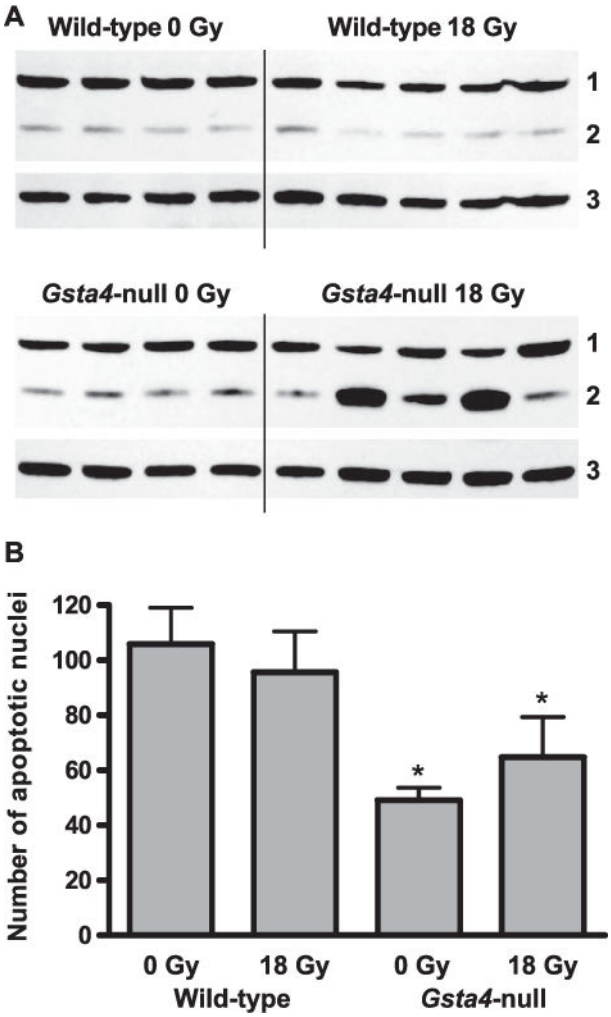

FIG. 3.

Cardiac markers of apoptosis determined 6 months after local heart irradiation. Panel A: Representative result of caspase-3 Western blot analysis. Row 1 shows caspase-3; row 2 shows cleaved caspase-3; and row 3 shows GAPDH loading control. In 3 out of 5 irradiated *Gsta4*-null mice, an increase was observed in left ventricular levels of cleaved caspase-3. Panel B: Numbers of apoptotic nuclei per heart section, determined from CardioTACS™ staining. Reduced numbers of apoptotic cells were seen in both sham-irradiated and irradiated *Gsta4*-null mice when compared to wild-type mice. Average ± SEM, n = 4–5. **P* < 0.05 when compared to wild-type sham-irradiated mice.

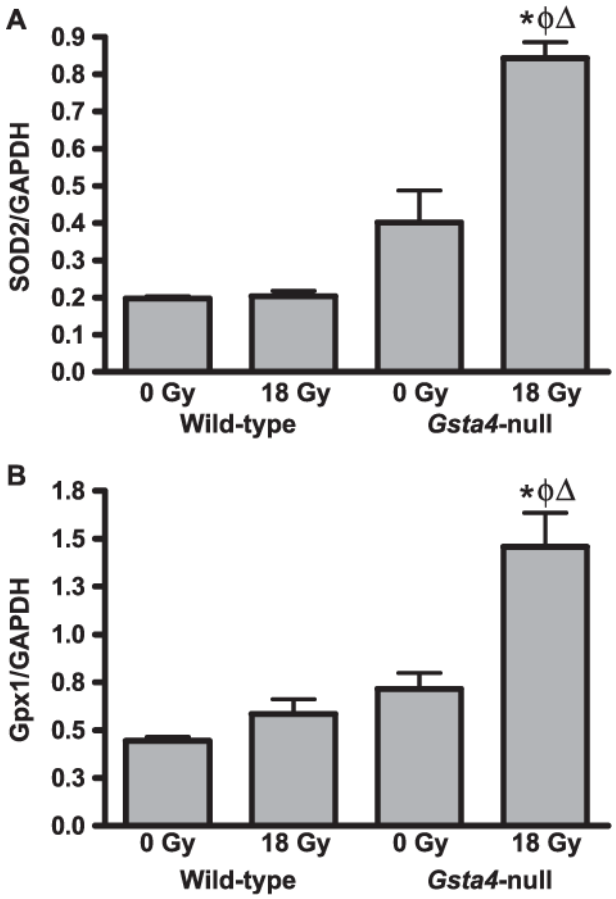

FIG. 4.

Left ventricular protein expression of SOD2 and Gpx1. Increased mRNA levels of the Nrf2 target genes *Sod2* (panel A) and *Gpx1* (panel B) in irradiated *Gsta4*-null mice (Table 1) coincided with increased left ventricular protein expression in these mice. Average ± SEM, n = 4–5. **P* < 0.05 when compared to wild-type sham-irradiated mice. φ*P* < 0.05 when compared to *Gsta4*-null sham irradiated. Δ*P* < 0.05 when compared to wild-type irradiated mice.

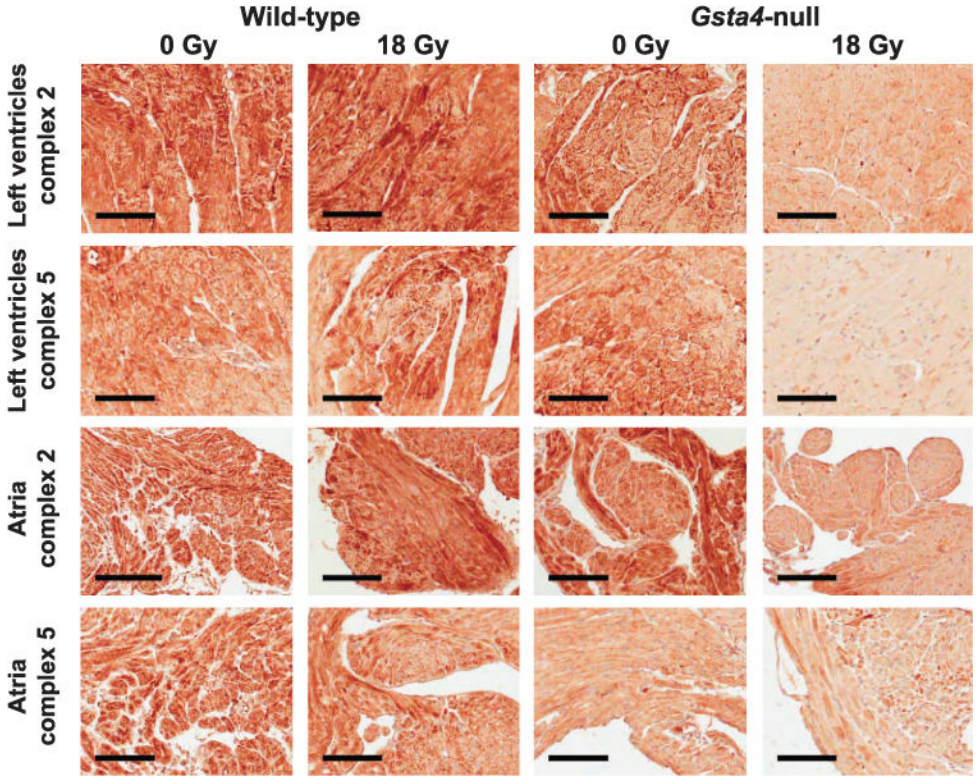

FIG. 5.

Cardiac tissue expression patterns of mitochondrial respiratory complexes 2 and 5 at 6 months after local heart irradiation. Representative images of complexes 2 and 5 immunohistochemistry of the left ventricles and atria of sham-irradiated and irradiated *Gsta4*-null and wild-type mice. Staining patterns were reduced in irradiated *Gsta4*-null mice. Scale bars indicate 100 μm.

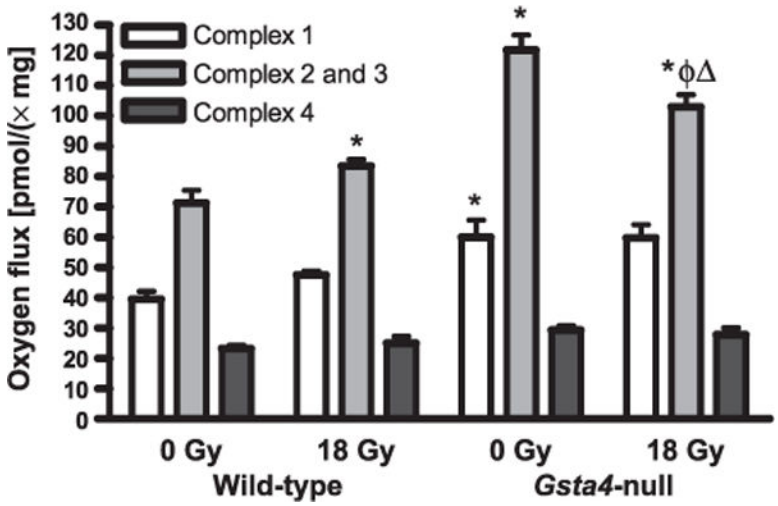

FIG. 6.

Oxygen flux measured in left ventricular tissue samples isolated at 6 months after local heart irradiation. In sham-irradiated mice, oxygraph measurements revealed a significantly higher oxygen flux through complexes 1, 2 and 3 in *Gsta4*-null compared to wild-type mice. Although exposure to radiation caused a reduction in oxygen flux through complexes 2 and 3 in *Gsta4*-null mice, the oxygen flux was still significantly higher compared to that in irradiated wild-type mice. Average ± SEM, n = 4. **P* < 0.05 when compared to wild-type sham-irradiated mice. φ*P* < 0.05 when compared to *Gsta4*-null sham-irradiated mice. Δ*P* < 0.05 when compared to wild-type irradiated mice.

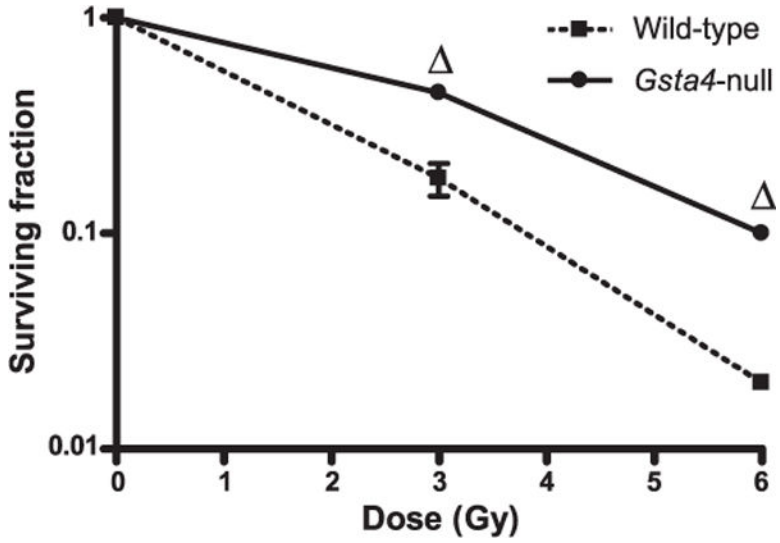

FIG. 7.

Mouse embryonic fibroblast survival in response to irradiation in culture. A clonogenic assay revealed a significantly higher postirradiation survival in mouse embryonic fibroblasts isolated from *Gsta4*-null mice compared to those isolated from wild-type mice. Average ± SEM, n = 3. Δ$P < 0.05$ when compared to wild-type mice.

TABLE 1

Relative mRNA Levels of Nrf2, PGAM5 and Target Genes of the Nrf2 Pathway.

	Wild-type 0 Gy	Wild-type 18 Gy	*Gsta4*-null 0 Gy	*Gsta4*-null 18 Gy
Nrf2	1.00 ± 0.05	2.16 ± 0.40[a]	2.08 ± 0.28[a]	4.23 ± 0.16[a,b,c]
PGAM5	1.03 ± 0.12	1.50 ± 0.08	2.91 ± 0.19[a,c]	6.53 ± 0.76[a,b,c]
Catalase	1.02 ± 0.09	1.51 ± 0.15	1.46 ± 0.18	4.09 ± 0.92[a,b,c]
SOD1	1.04 ± 0.13	0.88 ± 0.10	0.75 ± 0.09	0.96 ± 0.13
SOD2	1.01 ± 0.06	1.77 ± 0.34	1.95 ± 0.20	4.22 ± 0.49[a,b,c]
Peroxiredoxin 6	1.06 ± 0.16	1.68 ± 0.18	1.96 ± 0.27	3.12 ± 0.54[a,b,c]
Pyridoxal reductase (AKR8)	1.06 ± 0.17	1.36 ± 0.33	1.09 ± 0.14	1.26 ± 0.29
GPX1	1.02 ± 0.10	1.73 ± 0.31	2.00 ± 0.36	5.10 ± 0.51[a,b,c]
GSTA-1 and 2	1.06 ± 0.17	1.43 ± 0.17	2.23 ± 1.12	3.40 ± 0.64
GSTA-3	1.05 ± 0.16	0.88 ± 0.10	0.85 ± 0.12	1.69 ± 0.83
GSTM1	1.11 ± 0.26	1.28 ± 0.14	3.38 ± 0.49	5.72 ± 1.71[a,c]
Aldehyde ferredoxin oxidoreductase (AOR)	1.11 ± 0.22	1.78 ± 0.19	2.21 ± 0.38[a]	2.47 ± 0.35[a]
Glutamate-cysteine ligase, catalytic subunit (GCLC)	1.01 ± 0.09	1.47 ± 0.14	2.64 ± 0.36[a,c]	5.07 ± 0.32[a,b,c]
Glutamate-cysteine ligase, modifier subunit (GCLM)	1.06 ± 0.17	1.25 ± 0.22	0.72 ± 0.11[c]	0.96 ± 0.15
GPX4	1.02 ± 0.10	2.72 ± 0.32	1.69 ± 0.25	5.15 ± 1.24[a,b,c]
Thioredoxin reductase 1	1.05 ± 0.16	1.23 ± 0.06	1.09 ± 0.05	1.92 ± 0.05[a,b,c]

Notes. Real-time PCR-derived C_t values were used to calculate mRNA levels relative to wild-type sham-irradiated control. Average ± SEM, n = 5.

[a] $P < 0.05$ when compared to wild-type sham-irradiated mice.

[b] $P < 0.05$ when compared to *Gsta4*-null sham-irradiated mice.

[c] $P < 0.05$ when compared to wild-type irradiated mice.